Hindawi
Wireless Communications and Mobile Computing
Volume 2022, Article ID 4851364, 14 pages
https://doi.org/10.1155/2022/4851364

Research Article

Evolutionary Heuristic Computing Paradigm for 2D-DOA Estimation along Circular Array

Fiaz Hussain Shah,[1] Muhammad Asif Zahoor Raja,[2] Fadi Al-Turjman,[3] Fawad Zaman,[4] and Xiaodong Yang[1]

[1]*School of Electronic Engineering, Xidian University, Xi'an 710071, China*
[2]*Department of Electrical and Computer Engineering, COMSATS University Islamabad, Attock Campus, Attock 43600, Pakistan*
[3]*Artificial Intelligence Engineering Department, Research Centre for AI and IoT, Near East University, 99138 Nicosia, Mersin 10, Turkey*
[4]*Department of Electrical & Electronic Engineering, Imperial College London, UK*

Correspondence should be addressed to Xiaodong Yang; xdyang@xidian.edu.cn

Received 3 October 2021; Revised 21 November 2021; Accepted 6 April 2022; Published 30 April 2022

Academic Editor: Muhammad Asghar Khan

Direction of arrival (DOA) estimation problem has growing interest for the researcher investigating in system identification models arising in the field of digital signal processing, mobile communication, controls, and beamforming. In the presented work, evolutionary heuristic computing paradigm is presented for 2D-DOA estimation of plane waves impinging on uniform circular array. Performance metric of mean squared error is utilized as construction of a fitness function for the system, and the optimization strength of three methodologies, genetic algorithms (GAs), Pattern Search (PS), and integration of GAs with PS (GA-PS) is exploited for 2D-DOA estimation based on elevation as well as azimuth angles. Consistent precision, convergence, stability, and robustness of integrated heuristics of GA-PS are endorsed through outcomes of statistical observations.

1. Introduction

The use of different antenna structural arrays has growing interest in researchers due to remarkable performance in the domain of direction-of-arrival (DOA) parameter estimation, beamforming, radars, sonars, and seismology. Researchers proposed different DOA estimation procedures including MUSIC [1, 2], ESPRIT [3, 4] spatial smoothing methods [5, 6], subspace smoothing procedures [7], and temporal smoothing approach [8] for uniform linear array (ULA). The two-dimensional (2D) DOA (2D-DOA) estimation one preferred to used two-dimensional arrays based on L-shaped array [9, 10], nested array [11–13], coprime array [14, 15], uniform rectangle array (URA) [16, 17], uniform circular array (UCA) [18, 19], virtual uniform-linear-like array (VULA) [20], and visual array VT-MUSIC algorithm [21]. The transformation procedure also exploited for two-dimensional DOA (2D-DOA) estimation algorithms with relatively low computational requirement including UCA-RB-MUSIC [22], UCA-ESPRIT [23], UCA rank reduction [24], and root-MUSIC approach [25]. Beside these deterministic techniques for 1D and 2D DOA estimation, the stochastic procedures are also adopted for these global search based optimization problems [26–29]. All the existing procedures adopted for system identification of DOA models motivate

authors to investigate stochastic optimization mechanism by exploitation of evolutionary heuristics for joint estimation of two-dimensional DOA parameters impinging on circular structural array of far field sources.

The stochastic optimization mechanism by exploitation of artificial intelligence techniques has been implemented extensively to address constrained and unconstrained optimization model associated with a variety of linear/nonlinear systems [30–33]. Few prevailing recent applications include Hammerstein nonlinear control autoregressive systems, active noise control system, transport model for soft tissues, nonlinear optics, nonlinear Bratu systems, nonlinear fractional Riccati systems, nonlinear Jeffery-Hamel flow, nonlinear prey-predator, nonlinear thin film flow models, nonlinear FalknarSkan system, nonlinear Troesch problem, nonlinear singular Lane-Emden systems, nonlinear Thomas-Fermi model of atom, piezoelectric model, magneto-hydrodynamics, astrophysics, atomic physics, plasma physics, control, signal processing, energy, bioinformatics, economics, and finance (see references [34–36] and citation therein). These are source of incitements for authors to perform exploration and exploitation in evolutionary computational heuristic paradigm reliable treatment of 2-D DOA estimation of plane waves impinging of UCA.

In this paper, stochastic optimization solvers are presented for 2D-DOA estimation impinging on UCA from far field sources. The salient features of the scheme are highlighted as follows:

A novel application of evolutionary computational heuristic paradigm is presented for two-dimensional DOA estimation of far field sources involving uniform circular array by exploitation of global search efficacy of genetic algorithms (GAs), pattern search (PS), and integrated strength of GA-PS algorithms.

The performance of optimization mechanisms is substantiated by effective implementation of uniform circular array-based DOA estimation problem having different degrees of freedom. The results of integrated solver GA-PS are relatively better from standalone counterparts GA and PS for each scenario of the data model for DOA.

Consistent accuracy and convergence of the hybrid optimization scheme GA-PS are endorsed through outcomes of statistical observations for DOA problems with different numbers of decision variables and noise variations.

Organization of remaining of the paper is as follows. The data model for two-dimensional DOA estimation problem with uniform circular array geometry is presented in Section 2. Optimization methodology of all three algorithms is described in Section 3. The results of simulations through enough graphical and numerical illustrations with necessary interpretations are presented in Section 4. While the conclusions and further work are provided in last Section 5.

2. Data Model: 2D-DOA Estimation with UCA

When the data or system model for 2D-DOA estimation of plane waves impinging on UCA is presented here, the

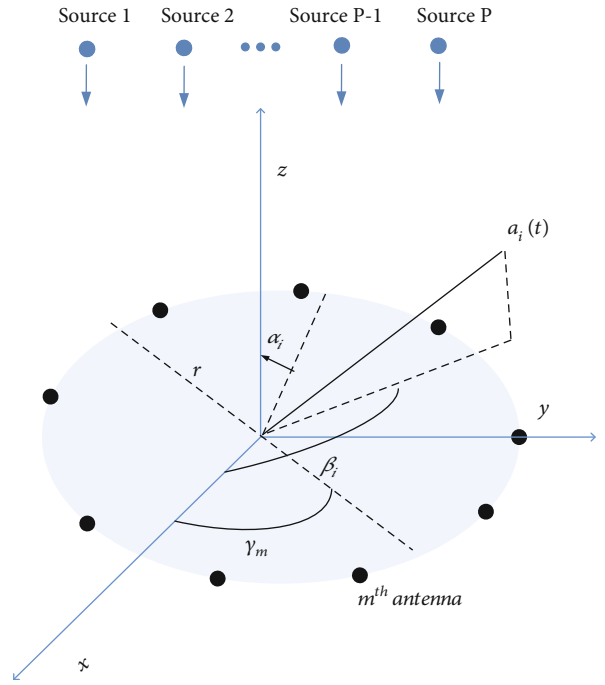

Figure 1: UCA geometry for plane waves.

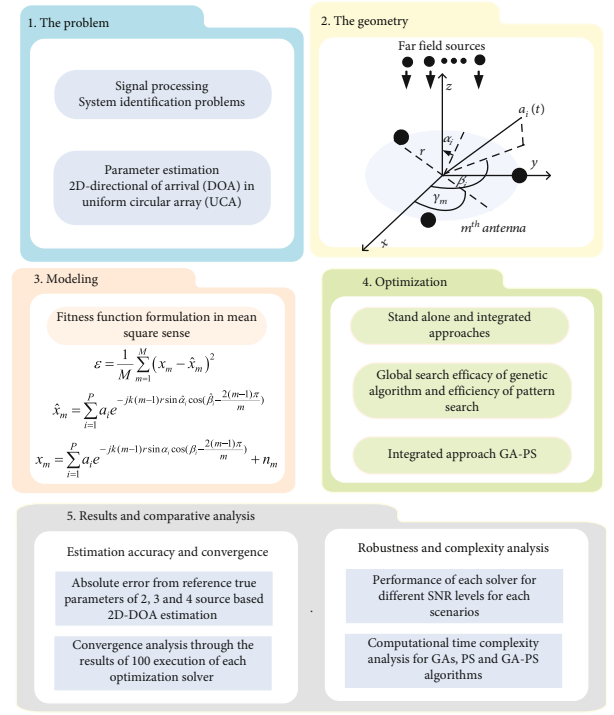

Figure 2: Block structure representation of workflow of the system.

UCA with M antennas have the angle of elevation α between 0 and $\pi/2$ and azimuth β between 0 and 2π for P far field sources, while the angle $\gamma_m = 2\pi m/M$ between mth antenna element for m between 0 and M-1 as shown in Figure 1.

Each electric field signal of m^{th} antenna in UCA from i^{th} sources is written as

$$E(r_m, t) = a_i(t)\mathrm{e}^{j\omega(t-d_i \cdot r_m)}, \quad \text{for } r_m = (x_m, y_m, z_m) = (r\sin(\beta_m), r\cos(\beta_m), 0), \tag{1}$$

where ω denotes the frequency, a_i be the i^{th} amplitude and d_i be i^{th} propagation direction at instance t. The relation for d_i in polar coordinates is given as

$$d_i = \frac{1}{c}(\sin\alpha_i \cos\beta_i, \sin\alpha_i \sin\beta_i, \cos\alpha_i). \tag{2}$$

Then,

$$d_i \cdot r_m = \frac{r}{c}\sin\alpha_i \cos(\beta_i - \gamma_m). \tag{3}$$

Equation (1) becomes

$$\begin{aligned} E(r_m, t) &= a_i(t)e^{j\omega(t-(r/c)\sin\alpha_i \cos(\beta_i-\gamma_n)} \\ &= a_i(t)\mathrm{e}^{j\omega t}\mathrm{e}^{-j(\omega r/c)\sin\alpha_i \cos(\beta_i-\gamma_m)}, \end{aligned} \tag{4}$$

for $A_i(t) = a_i(t)\mathrm{e}^{j\omega t}$ and $k = \omega/c = 2\pi/\lambda$; we get

$$E(r_m, t) = A_i(t)e^{-jkr(m-1)\sin\alpha_i \cos(\beta_i-\gamma_m)}. \tag{5}$$

In case of response, $x_m(t) = E(r_m, t)$ of m^{th} antenna of UCA with noise $n_m(t)$ is given as

$$x_m(t) = \sum_{i=1}^{P} a_i(t)e^{-jk(m-1)r\sin\alpha_i \cos(\beta_i-((2(m-1)\pi)/m))} + n_m(t). \tag{6}$$

The response for single snapshot is given as

$$x_m = \sum_{i=1}^{P} a_i e^{-jk(m-1)r\sin\alpha_i \cos(\beta_i-((2(m-1)\pi)/m))} + n_m. \tag{7}$$

In a matrix form, the response of UCA can be written as follows:

$$\begin{bmatrix} x_1 \\ x_2 \\ \vdots \\ x_M \end{bmatrix} = \begin{bmatrix} 1 & 1 & \cdots & 1 \\ e^{-jkr\sin\alpha_1 \cos(\beta_1-\pi)} & e^{-jkr\sin\alpha_2 \cos(\beta_2-\pi)} & \cdots & e^{-jkr\sin\alpha_p \cos(\beta_p-\pi)} \\ \vdots & \vdots & \vdots & \vdots \\ -jkr(m-1)\sin\alpha_1 \cos\left(\beta_1 - \dfrac{2\pi(m-1)}{m}\right) & e^{-jkr(m-1)\sin\alpha_1 \cos\left(\beta_2-\frac{2\pi(m-1)}{m}\right)} & \cdots & e^{-jkr\sin\alpha_p \cos\left(\beta_p-\frac{2\pi(m-1)}{m}\right)} \end{bmatrix} \begin{bmatrix} a_1 \\ a_2 \\ \vdots \\ a_p \end{bmatrix} + \begin{bmatrix} n_1 \\ n_2 \\ \vdots \\ n_m \end{bmatrix}. \tag{8}$$

In a vector form, equation (8) is given as

$$\mathbf{x} = \mathbf{A}\mathbf{s} + \mathbf{n}. \tag{9}$$

Here, $\mathbf{s}$ is a steering matrix for the source signals, a matrix $\mathbf{A}$ for amplitude and noise signal is denoted by $\mathbf{n}$.

3. Design Methodology

The design methodology consisted of two parts: a fitness function formulation for 2D-DOA parameter estimation and its optimization with the help of genetic algorithms (GA), pattern search (PS) and integrated approach GA-PS. The generic flow diagram of the proposed methodology is shown in Figure 2.

3.1. Fitness Function of 2D-DOA Estimation of UCA. The fitness function is developed for 2D-DOA estimation of plane waver form P sources impinging on circulate array compose of M antenna elements by the proficiency of approximation theory in mean square error sense as follows:

$$\varepsilon = \frac{1}{M}\sum_{m=1}^{M}(x_m - \widehat{x}_m)^2, \tag{10}$$

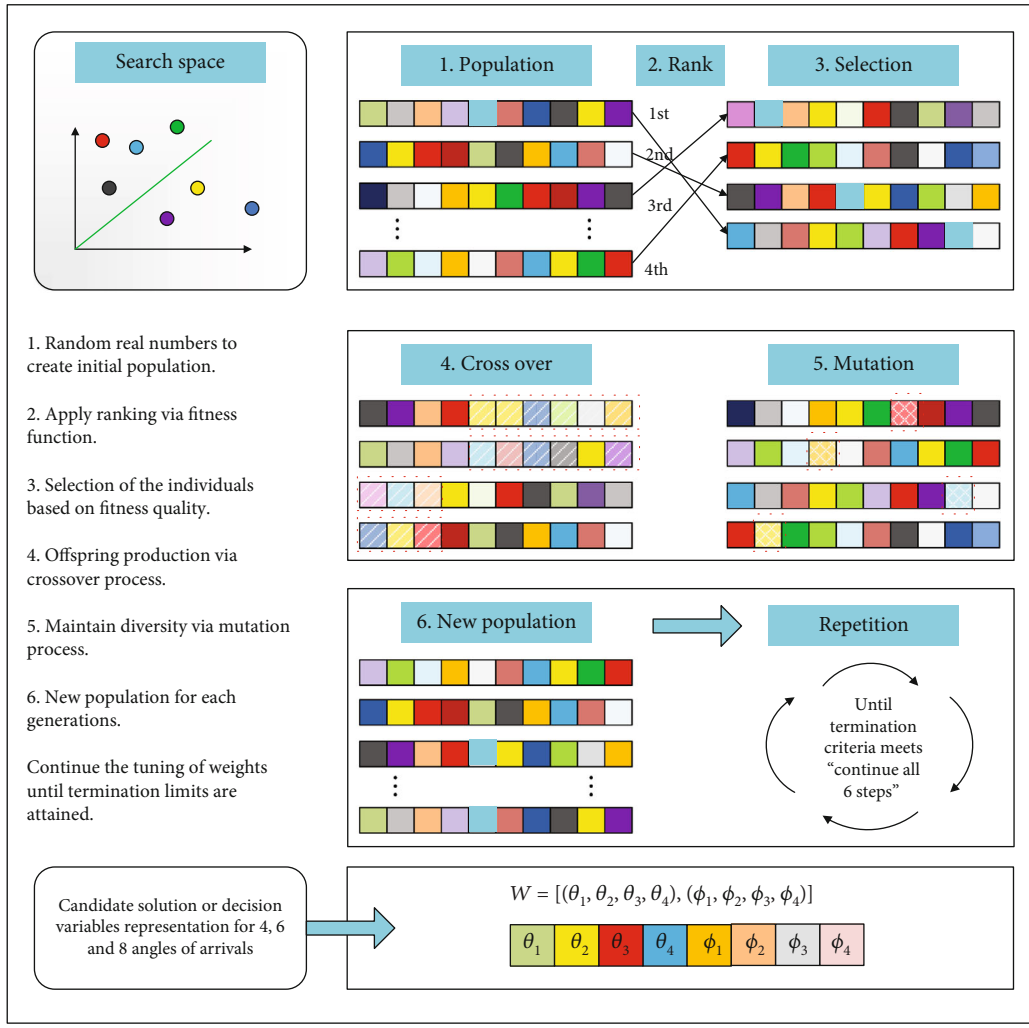

Figure 3: Optimization cycle of genetic algorithms.

where

$$x_m = \sum_{i=1}^{P} a_i e^{-jk(m-1)r \sin \alpha_i \cos (\beta_i - ((2(m-1)\pi)/m))} + n_m,$$
$$\hat{x}_m = \sum_{i=1}^{P} a_i e^{-jk(m-1)r \sin \widehat{\alpha}_i \cos \left(\widehat{\beta}_i - ((2(m-1)\pi)/m)\right)}. \quad (11)$$

Here, x_m is the desired response or signal in case of single snapshot as given equation (7), while $\hat{x}_m$ is an approximate signal of x_m. Now, one has to find the appropriate weights as

$$W = (\alpha_1, \alpha_2, \cdots, \alpha_P, \beta_1, \beta_2, \cdots, \beta_P), \quad (12)$$

such that $\varepsilon \longrightarrow 0$; then accordingly, $\hat{x}_m \longrightarrow x_m$.

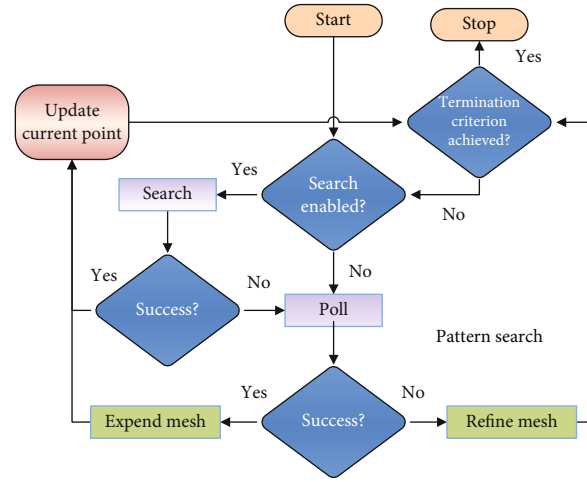

Figure 4: Process flow diagram of PS algorithm.

Table 1: Settings for gas optimization tools.

Index	Set
Individuals in population	360
Total number of generations	1000
Crossover scheme	Heuristic routine
Fraction of crossover	0.2
Function tolerance	10-09
Range initialization	[0-2π]
Selection scheme	Routine of stochastic uniform
Scaling procedure	Ranking
Elitism	2 counts
Mutation scheme	Routine of adaptive feasible
Other	Defaults

Table 2: Settings for PS optimization tools.

Index	Set
Iterations	2000
Penalty	100
Polling scheme	GPS basis on 2 N
Poll ordering	Consecutive
Mesh size	02
Evaluation of fitness	200000
Expansion parameter	2
Contraction parameter	0.5
TolX	0
TolBind	0
TolMesh	10-09

3.2. Optimization of 2D-DOA Parameters. To find the unknown adjustable weights W, 2D-DOA parameter estimation, the standalone optimization strength of GAs, and PS method, as well as hybrid computing heuristics of GA-PS algorithm, are exploited.

GA is developed on mathematical modeling of natural genetic mechanism in human genetic system and the first renewed application introduced by Onnen [37] in early seventies of the last century. GAs work through its fundamental operators of selection, crossover, and mutation for reproduction of the new population of candidate solution at each step increment in generations. The generic workflow of GAs operations is illustrated in Figure 3, while further necessary details of processing blocks can be seen in [38, 39]. Many constrained and unconstrained nonlinear optimization problems are effectively addressed with competency of GAs such as optimization in filter designing [40], life prediction of supercapacitors [41], salesman problem [42], multiaccess edge computing [43], and multiobjective optimization [44].

A pattern search algorithm belongs to the class of derivative free algorithm used broadly by the researchers for viable solution of constrained and unconstrained optimization tasks [45, 46]. The generic workflow diagram of PS by means of process block structures is shown in Figure 4, while broad recent applications of PS in different fields of science and engineering include the design of PID controller [47], automotive safety [48], and health monitoring [49].

In the presented study, standalone and combine strength of both optimization algorithms based on GAs, PS, and GA-PS are used for 2D-DOA estimation of plane waves. The built-in routines are invoked for both GAs and PS methods using the optimization toolbox of MATLAB software with setting of GAs and PS tools as provided in Tables 1 and 2, respectively.

4. Simulations and Results

In this section, results with interpretations are presented for abundant experimentation to test, analyze, and compare the outcomes of GAs PS and GA-PS based on the proposed methodologies. Results are presented throughout in this study based on average of 100 independent trials.

To evaluate the performance of GAs, PS, and their integrated scheme GA-PS, three case studies are taken based on 2, 3, and 4 plane wave sources impinging of UCA as follows:

Case 1. In the said scenario, 2D-DOA estimation problem with $P = 2$ sources and $M = 6$ antenna elements on UCL is taken with settings of elevation α_1 and azimuth β_1 angles as follows:

$$W = (\alpha_1, \alpha_{2,}\beta_1, \beta_2) = \begin{cases} (20^\circ, 70^\circ, 110^\circ, 150^\circ) \text{ degrees}, \\ (0.3491, 1.2217, 1.9199, 2.6180) \text{ radians}, \end{cases} \quad (13)$$

while the values of amplitude are $a = [a_1, a_2] = [1, 3]$. The fitness function for case 1 with $P = 2$ and $M = 6$ is formulated as follows:

$$\varepsilon = \frac{1}{6}\sum_{m=1}^{6}(x_m - \widehat{x}_m)^2,$$

$$x_m = \sum_{i=1}^{2} a_i e^{-jk(m-1)r \sin \alpha_i \cos (\beta_i - ((2(m-1)\pi)/m))} + n_m,$$

$$\widehat{x}_m = \sum_{i=1}^{2} a_i e^{-jk(m-1)r \sin \widehat{\alpha}_i \cos \left(\widehat{\beta}_i - (2(m-1)\pi)/m\right)}. \quad (14)$$

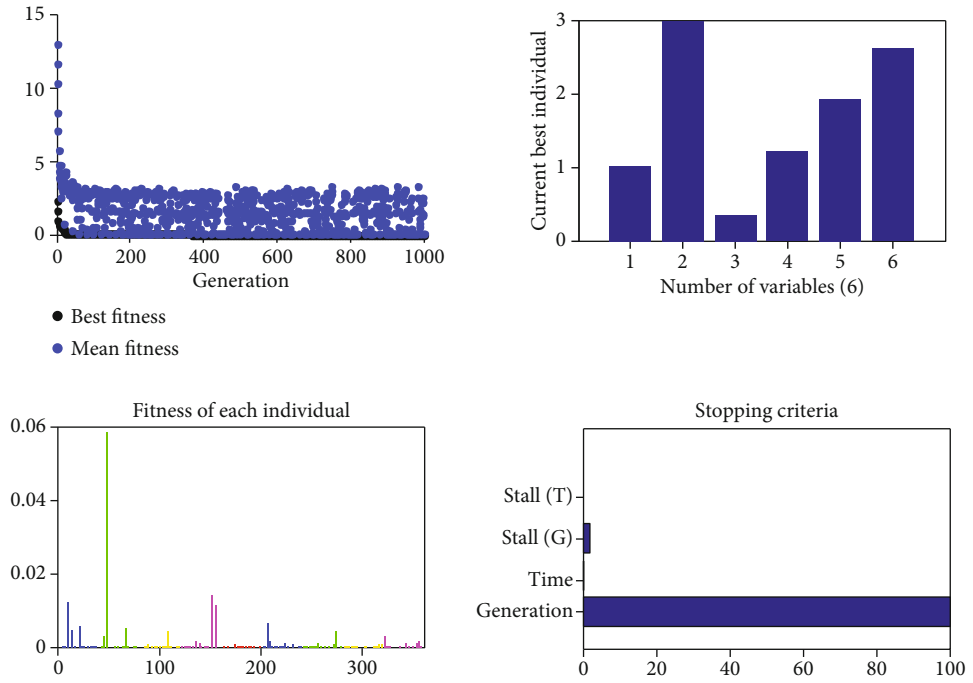

Figure 5: Learning curve with global best individual, fitness of each individual, and stopping conditions of GAs for case 1 of 2D-DOA estimation.

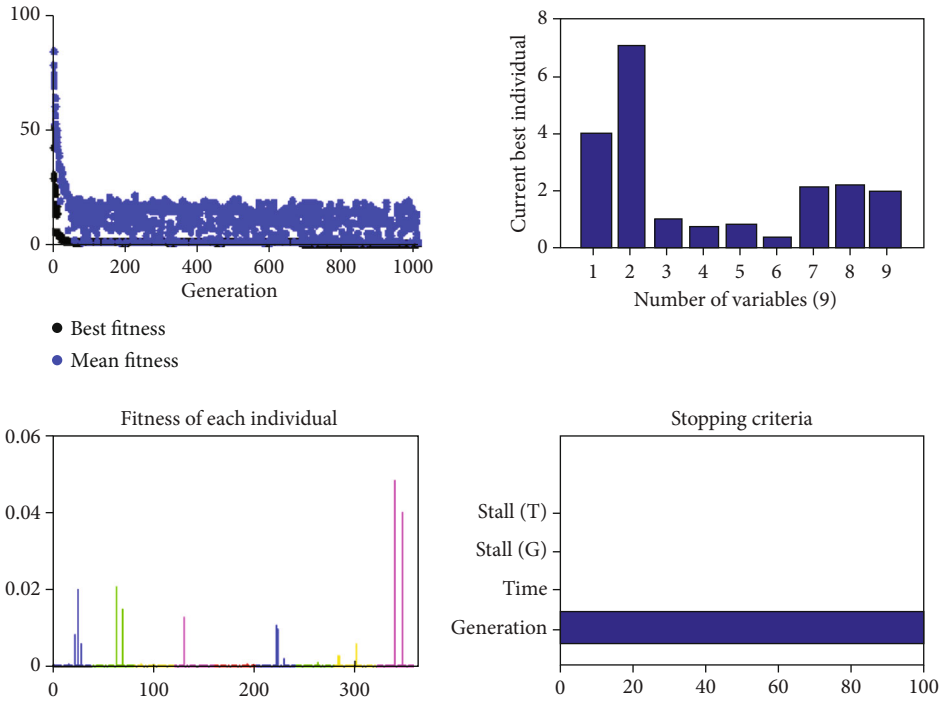

Figure 6: Learning curve with the best global individual, fitness of each individual, and stopping conditions of GAs for case 2 of 2D-DOA estimation.

Table 3: Comparison of results for 2D-DOA model for 2 far field sources.

Index	Desire and Approximated parameters			
	$\alpha 1$	$\alpha 2$	$\beta 1$	$\beta 2$
True (deg)	20.0000	70.0000	110.0000	150.0000
True (rad)	0.3491	1.2217	1.9199	2.6180
GAs (deg)	19.9962	69.9925	109.9964	149.9946
GAs(rad)	0.3490	1.2216	1.9198	2.6179
PS (deg)	19.9905	69.9868	109.9850	149.9889
PS (rad)	0.3489	1.2215	1.9196	2.6178
GA-PS (deg)	20.0020	69.9983	110.0022	150.0004
GA-PS (rad)	0.3491	1.2217	1.9199	2.6180

Table 4: Comparison of results for 2D-DOA model for 3 far field sources.

Index	Parameters					
	$\alpha 1$	$\alpha 2$	$\alpha 3$	$\beta 1$	$\beta 2$	$\beta 3$
True (deg)	20.0000	40.0000	50.0000	110.000	120.000	125.000
True (rad)	0.3491	0.6980	0.8727	1.9190	2.0944	2.1817
GAs (deg)	19.9962	39.9925	49.9791	109.6469	119.9946	124.9850
GAs (rad)	0.3490	0.6980	0.8723	1.9137	2.0943	2.1814
PS (deg)	19.9767	39.9649	49.9475	109.4138	119.9348	124.9290
PS (rad)	0.3488	0.6978	0.8721	1.9104	2.0941	2.1813
GA-PS (deg)	20.0020	39.9925	50.0020	109.9506	120.0003	125.0022
GA-PS (rad)	0.3491	0.6980	0.8727	1.9190	2.0944	2.1817

Table 5: Comparison of results for 2D-DOA model for 4 far field sources.

Index	Desire and Approximated parameters							
	Elevation angle				Azimuth angle			
	$\alpha 1$	$\alpha 2$	$\alpha 1$	$\alpha 2$	$\beta 1$	$\beta 1$	$\beta 1$	$\beta 1$
True (deg)	20.000	54.000	62.000	35.000	105.000	133.000	125.000	166.000
True (rad)	0.3491	0.9424	1.0821	0.6108	1.8325	2.3212	2.1816	2.8972
Gas (deg)	19.939	53.967	61.960	34.996	104.966	132.978	124.979	165.974
Gas (rad)	0.3480	0.9419	1.0814	0.6108	1.8320	2.3209	2.1813	2.8968
PS (deg)	19.933	53.950	61.977	34.996	104.960	132.972	124.968	165.951
PS (rad)	0.3479	0.9416	1.0817	0.6108	1.8319	2.3208	2.1811	2.8964
GA-PS (deg)	19.990	53.978	61.994	34.996	104.983	132.984	124.991	165.986
GA-PS (rad)	0.3489	0.9421	1.0820	0.6108	1.8323	2.3210	2.1815	2.8970

Table 6: Comparative study 2D-DOA model for 2 far field sources.

Index	Noise (dB)	ε	Time	Gens/iter	FC
GAs	Nil	$4.03E-25$	43.12	1000	360360
	30	$3.39E-22$	43.04	1000	360360
	25	$5.61E-19$	43.92	1000	360360
	20	$3.79E-18$	44.14	1000	360360
	15	$6.96E-18$	44.69	1000	360360
	10	$4.19E-17$	45.01	1000	360360
	5	$9.68E-16$	48.50	1000	360360
PS	Nil	$7.26E-21$	3.79	2000	23507
	30	$1.34E-21$	3.80	2000	23507
	25	$4.79E-19$	3.93	2000	23231
	20	$6.26E-18$	3.83	2000	23145
	15	$5.58E-16$	3.85	2000	23468
	10	$4.63E-15$	3.85	2000	23277
	5	$1.89E-14$	3.86	2000	23601
GA-PS	Nil	$1.00E-00$	46.70	3000	383867
	30	$1.00E-34$	46.63	3000	380576
	25	$6.42E-31$	47.53	3000	383591
	20	$1.71E-30$	47.75	3000	381109
	15	$6.23E-28$	48.31	3000	381010
	10	$2.54E-26$	48.64	3000	381359
	5	$1.85E-26$	52.16	3000	381469

Case 2. In this case, 2D-DOA estimation problem with $P = 3$ sources and $M = 9$ antenna elements on UCL is taken with settings of elevation α_1 and azimuth β_1 angles in degree or radian as follows:

$$W = (\alpha_1, \alpha_{2,}\alpha_{3,}\beta_1, \beta_2, \beta_3) = \begin{cases} \begin{pmatrix} 20^\circ, & 40^\circ, & 50^\circ, \\ 110^\circ, & 120^\circ, & 125^\circ \end{pmatrix} \text{degrees}, \\ \begin{pmatrix} 0.3491, 0.6980, 0.8727, \\ 1.9190, 2.0944, 2.1817 \end{pmatrix} \text{radians}, \end{cases} \tag{15}$$

while the values of amplitude are $a = [a_1, a_2, a_3] = [1, 4, 7]$. Using equation (14) for $P = 3$ and $M = 9$, the fitness function for case 2 is constructed.

Case 3. In this scenario, 2D-DOA estimation problem with $P = 4$ sources and $M = 8$ antenna elements on UCL is taken with settings of elevation α and azimuth β angles as follows:

$$W = \begin{pmatrix} \alpha_1, \alpha_{2,}\alpha_{3,} \\ \beta_1, \beta_2, \beta_3 \end{pmatrix} = \begin{cases} \begin{pmatrix} 20^\circ, & 40^\circ, & 50^\circ, \\ 110^\circ, & 120^\circ, & 125^\circ \end{pmatrix} \text{degrees}, \\ \begin{pmatrix} 0.3491, 0.6980, 0.8727, \\ 1.9190, 2.0944, 2.1817 \end{pmatrix} \text{radians}, \end{cases} \tag{16}$$

while the values of amplitude are $a = [a_1, a_2, a_3, a_3] = [1]$. Using equation (7) for $P = 4$ and $M = 8$, the fitness function for case 3 is constructed.

Results are determined for 100 independent trials of the algorithms to pinpoint their performance for two, three, and four far field sources. The optimization characteristics of GAs for 2 and 3 source models in terms of learning curves, best individual, fitness of each individual in the population, and stoppage criteria are shown in Figures 5 and 6 in case of 2 and 3 far-field sources impinging on UCL.

Table 7: Comparative study 2D-DOA model for 3 far field sources.

Index	Noise (dB)	ε	Time	Gens/iter	FC
GAs	Nil	$1E-21$	55.1	1000	360360
	30	$2E-20$	56.4	1000	360360
	25	$3E-19$	56.7	1000	360360
	20	$5E-18$	58.3	1000	360360
	15	$8E-17$	59.4	1000	360360
	10	$9E-16$	60.1	1000	360360
	5	$9E-14$	62.3	1000	360360
PS	Nil	$7.E-15$	5.4	2000	35660
	30	$1E-15$	5.7	2000	35876
	25	$4.E-14$	6.4	2000	35897
	20	$7E-12$	6.7	2000	35876
	15	$4E-10$	6.7	2000	35879
	10	$2E-8$	6.8	2000	35956
	5	$2E-6$	6.9	2000	35989
GA-PS	Nil	$2E-28$	60.20	3000	386246
	30	$2E-28$	61.80	3000	386281
	25	$5E-26$	62.30	3000	386732
	20	$2E-24$	64.10	3000	387149
	15	$6E-24$	65.30	3000	387257
	10	$2E-22$	66.00	3000	387485
	5	$2E-20$	68.40	3000	387681

The results of all three algorithms GAs, PS, and GA-PS against the true parameters of 2, 3 and 4 far-field sources for noiseless environment are presented in Tables 3–5, respectively.

While in case of different noise levels, results of proposed computing paradigm are presented in Tables 6–8 for sources $P = 2$, 3, and 4, respectively. The values of fitness ε and complexity parameters are time consumed, generations/iterations (Gens/iter) executed, and fitness function counts (FCs) by the optimization strategy for finding the decision variables.

One may observe that all three methods attained reasonably well levels of estimation accuracy; however, the results of integrated computing heuristics of GA-PS are more precise than those of GAs and PS standalone solvers. The performance of integrated algorithm GA-PS at the expense of relatively more computations is better than that of standalone schemes. Additionally, the increase in the number of sources and the level of noise variances results are deteriorated for each computing algorithm GAs, PS, and GA-PS, but still, the hybrid GA-PS achieved better reasonable precision than that of standalone counterparts.

The convergence analysis is also conducted for all three optimization solvers GAs, PS and GA-PS for solving 2D-DOA estimation problems are based on 100 trails, and results are presented in Figure 7 and Table 9 for each case study. One may see that percentage convergence of integrated heuristic of GA-PS algorithm is higher from standalone methodologies and performance of each optimization solver degraded with increase in sources from 2 to 4.

The analysis is further conducted with the increase in the number of antenna elements in UCA, i.e., value of M. The results of convergence analysis of 2D-DOA estimation for $P = 2$ and $M = 6$, 8, and 10 in UCL are presented in Table 10 along with achieved fitness level for all three optimization schemes. Accordingly, the results of convergence analysis of 2D-DOA estimation for 3 and 4 far-field sources with different antenna elements in UCA are presented in Tables 11 and 12, respectively. It is seen that rate of convergence for each algorithm increases with the increase in the value of M, but the performance of hybridized approach GA-PS is better from the rest.

Robustness analysis of all three optimization methodologies is conducted for different values of signal to noise (SNR), i.e., 5 dB, 10 dB, 15 dB, 20 dB, 25 dB, and 30Db for 2D-DOA estimation of 2, 3, and 4 sources. The results of robustness analysis each algorithm for different noise variation are presented in Figures 8–10 for sources $P = 2$, 3, and 4, respectively. One may see that for both low and

Table 8: Comparative study 2D-DOA model for 4 far field sources.

Index	Noise (dB)	ε	Time	Gens/iter	FC
GAs	Nil	$6.3e-12$	66.5	1000	360360
	30	$1.2e-09$	66.8	1000	360360
	25	$6.7e-09$	69.8	1000	360360
	20	$8.3e-08$	69.3	1000	360360
	15	$8.9e-08$	71.1	1000	360360
	10	$1.8e-07$	72.3	1000	360360
	5	$1.9e-06$	72.5	1000	360360
PS	Nil	$3.2e-09$	7.2	2000	35660
	30	$2.7e-08$	7.7	2000	35876
	25	$7.3e-08$	7.8	2000	35897
	20	$2.9e-06$	7.9	2000	35876
	15	$1.8e-06$	8.6	2000	35879
	10	$1.9e-04$	8.7	2000	35956
	5	$8.2e-04$	8.9	2000	35989
GA-PS	Nil	$8.3e-16$	73.20	3000	386246
	30	$1.2e-14$	73.60	3000	386281
	25	$8.7e-14$	76.60	3000	386732
	20	$4.3e-12$	76.20	3000	387149
	15	$6.9e-12$	78.20	3000	387257
	10	$1.8e-10$	79.50	3000	387485
	5	$8.9e-09$	80.00	3000	388681

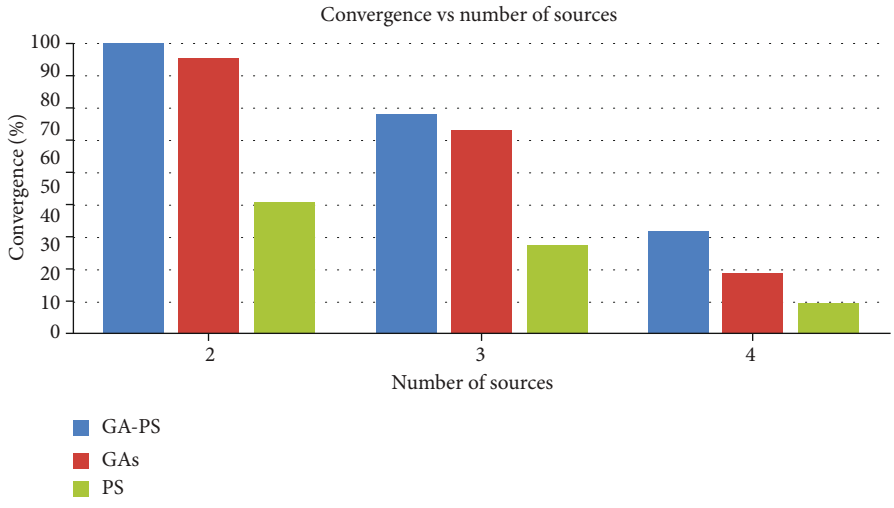

Figure 7: Bar chart illustration of convergence analysis for sources $P = 2$, 3, and 4.

Table 9: Convergence analysis of 2D-DOA estimation for 2, 3, and 4 far field sources with fixed antenna elements in UCL.

Source/antenna	Method	ε	Convergence
2/4	Gas	$1.0E-25$	94%
	PS	$1.0E-21$	44%
	GA-PS	$1.0E-31$	98%
3/6	GAs	$1.0E-21$	69%
	PS	$1.0E-15$	31%
	GA-PS	$1.0E-288$	76%
4/8	GAs	$1.0E-06$	19%
	PS	$1.0E-05$	09%
	GA-PS	$1.0E-17$	36%

Table 10: Convergence analysis of 2D-DOA estimation for 2 far field sources with different antenna elements in UCL.

Antenna UCA	Method	ε	Convergence
6	GAs	$1.0E-25$	95%
	PS	$1.0E-21$	45%
	GA-PS	$1.0E-31$	99%
8	GAs	$1.0E-27$	96%
	PS	$1.0E-22$	52%
	GA-PS	$1.0E-32$	99%
10	GAs	$1.0E-28$	98%
	PS	$1.0E-25$	60%
	GA-PS	$1.0E-00$	100%

Table 11: Convergence analysis of 2D-DOA estimation for 3 far field sources with different antenna elements in UCL.

Antenna UCA	Method	ε	Convergence
9	GAs	$1.0E-21$	69%
	PS	$1.0E-15$	29%
	GA-PS	$1.0E-28$	74%
11	GAs	$1.0E-22$	74%
	PS	$1.0E-16$	39%
	GA-PS	$1.0E-29$	82%
13	GAs	$1.0E-22$	77%
	PS	$1.0E-17$	43%
	GA-PS	$1.0E-30$	85%

Table 12: Convergence analysis of 2D-DOA estimation for 4 far field sources with different antenna elements in UCL.

Antenna UCA	Scheme	ε	Convergence (%)
8	GA	$1.0E-06$	20
	PS	$1.0E-03$	10
	GA-PS	$1.0E-08$	35
10	GA	$1.0E-07$	26
	PS	$1.0E-04$	18
	GA-PS	$1.0E-09$	45
12	GA	$1.0E-07$	30
	PS	$1.0E-05$	25
	GA-PS	$1.0E-10$	55

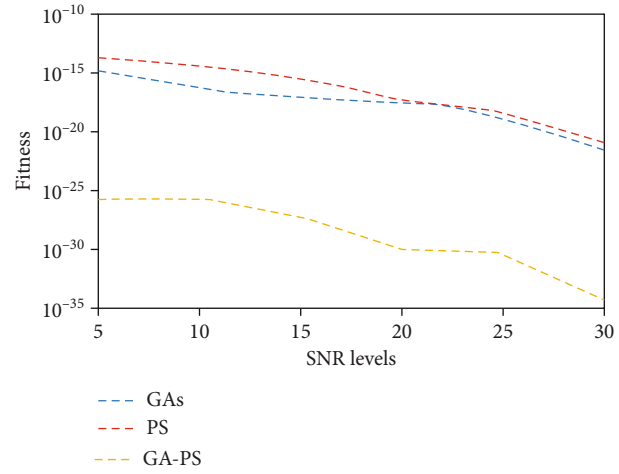

Figure 8: Comparison of fitness for different SNR levels for sources $P = 2$.

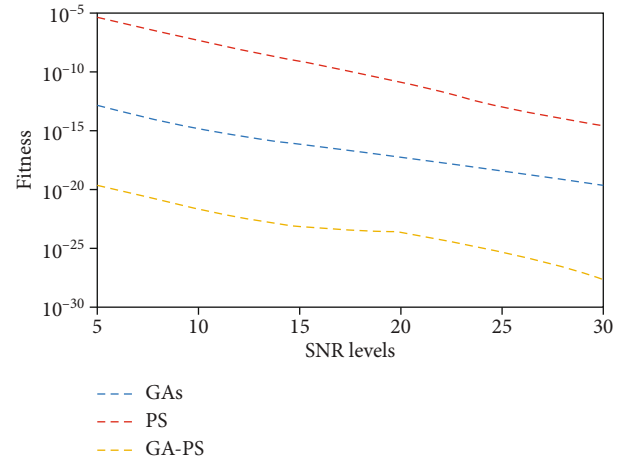

Figure 9: Comparison of fitness for different SNR levels for sources $P = 3$.

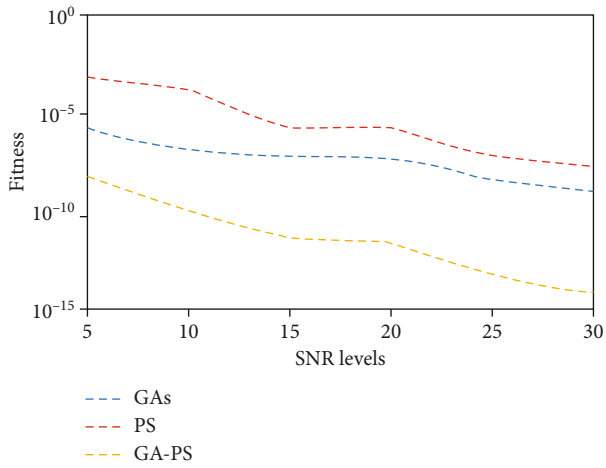

Figure 10: Comparison of fitness for different SNR levels for sources $P = 4$.

Table 13: Performance comparison on statistics for 2 sources based on 2D-DOA estimation.

Index	GAs	PS	GA-PS
Best-fitness	$1.0E-25$	$1.0E-23$	$1.0E-00$
Worst-fitness	$1.0E-21$	$1.0E-17$	$1.0E-28$
Mean-fitness	$1.0E-23$	$1.0E-21$	$1.0E-30$
Minimum-FCs	360360	20545	23147
Maximum-FCs	360360	21324	23986
Mean-FCs	360360	20777	23327
Minimum-time	42.52	3.69	46.10
Maximum-time	44.27	5.01	48.02
Mean-time	43.28	3.91	47.00

Table 14: Performance comparison on statistics for 3 sources based on 2D-DOA estimation.

Index	GAs	PS	GA-PS
Best-fitness	$1.0E-17$	$1.0E-12-12$	$1.0E-31$
Worst-fitness	$1.0E-13$	$1.0E-02$	$1.0E-18$
Mean-fitness	$1.0E-15$	$1.0E-06$	$1.0E-28$
Minimum-FCs	360360	25467	25538
Maximum-FCs	360360	28580	29614
Mean-FCs	360360	26339	26598
Minimum-time	53.09	4.71	58.20
Maximum-time	61.55	6.25	67.62
Mean-time	56.80	5.09	61.88

high values of SNR, the performance of hybridized computing solver GA-PS remains better than that of GAs and PS standalone schemes.

The complexity analysis in terms of minimum-time, maximum-time, mean-time, minimum-FCs, maximum-FCs, and mean-FCs along with the values of best-fitness, worst-fitness and mean-fitness is conducted for 100 executions of each optimization scheme GAs, PS, and GA-PS for all three 2D-DOA scenarios. Results of complexity operators are listed in Tables 13–15 for sources $P = 2$, 3, and 4, respectively. It is seen that computation complexity of PS is superior from GA and GA-PS technique but the performance in terms of accuracy and convergence is better for both GAs and GA-PS methodologies for each case.

Table 15: Performance comparison on statistics for 4 sources based on 2D-DOA estimation.

Index	GAs	PS	GA-PS
Best-fitness	$1.0E-12$	$1.0E-09$	$1.0E-16$
Worst-fitness	$1.0E-04$	$1.0E-01$	$1.0E-05$
Mean-fitness	$1.0E-11$	$1.0E-04$	$1.0E-15$
Minimum-FCs	360360	25347	25538
Maximum-FCs	360360	28720	29614
Mean-FCs	360360	26759	26598
Minimum-time	73.01	9.12	79.11
Maximum-time	69.55	7.51	76.45
Mean-time	72.01	7.83	78.71

5. Conclusion

Novel applications of evolutionary heuristics are effectively presented for 2D-DOA estimation of plane waves impinging on UCL by exploitation of global search efficacy of GAs, efficiency of PS, and integrated optimization strength of GA-PS. The performance of optimization mechanisms is verified by implementation of UCA-based 2D-DOA estimation having different degrees of freedom, i.e., far field sources $P = 2$, 3, and 4. The results of integrated solver GA-PS are relatively better from standalone counterparts GA and PS for each scenario of the data model for DOA. Consistent accuracy, stability, and robustness of the hybrid optimization procedure of GA-PS are established through outcomes of statistical observations for DOA problems with different numbers of decision variables and noise variations but at the cost of relative more computations that that of GAs and PS standalone schemes.

In the future, one may investigate the application of presented computing platform on other circular array structures based on concentric circular array, conic circular array, and coprime circular array for better estimation accuracy of DOA parameters. Moreover, the use of fractional evolutionary/swarming techniques looks promising for the estimation of 2D-DOA parameters more viably.

Data Availability

The data used to support the findings of this study are available from the corresponding author upon request.

Conflicts of Interest

The authors declare that they have no conflicts of interest.

Acknowledgments

The work was supported in part by the Fundamental Research Funds for the Central Universities (No. JB180205).

References

[1] H. Zhang and H. Zhang, "Research on DOA estimation method of sonar radar target based on MUSIC algorithm," *Journal of Physics: Conference Series*, vol. 1176, no. 3, 2019.

[2] X. Zhang, C. Chen, J. Li, and D. Xu, "Blind DOA and polarization estimation for polarization-sensitive array using dimension reduction MUSIC," *Multidimensional Systems and Signal Processing*, vol. 25, no. 1, pp. 67–82, 2014.

[3] J. Li, X. Zhang, W. Chen, and T. Hu, "Reduced-dimensional ESPRIT for direction finding in monostatic MIMO radar with double parallel uniform linear arrays," *Wireless Personal Communications*, vol. 77, no. 1, pp. 1–19, 2014.

[4] R. Roy and T. Kailath, "ESPRIT-estimation of signal parameters via rotational invariance techniques," *IEEE Transactions on Acoustics, Speech and Signal Processing*, vol. 37, no. 7, pp. 984–995, 1989.

[5] J. Dai and Z. Ye, "Spatial smoothing for direction of arrival estimation of coherent signals in the presence of unknown mutual coupling," *IET Signal Processing*, vol. 5, no. 4, pp. 418–425, 2011.

[6] C. Qi, Y. Wang, Y. Zhang, and Y. Han, "Spatial difference smoothing for DOA estimation of coherent signals," *IEEE Signal Processing Letters*, vol. 12, no. 11, pp. 800–802, 2005.

[7] S. Visuri, H. Oja, and V. Koivunen, "Subspace-based direction-of-arrival estimation using nonparametric statistics," *IEEE Transactions on Signal Processing*, vol. 49, no. 9, pp. 2060–2073, 2001.

[8] D. R. Van Rheeden and S. C. Gupta, "A temporal smoothing approach to direction of arrival estimation of coherent signals in fading channels," in *WCNC. 1999 IEEE Wireless Communications and Networking Conference (Cat. No.99TH8466)*, pp. 286–290, New Orleans, LA, USA, 1999.

[9] N. Xi and L. Liping, "A computationally efficient subspace algorithm for 2-D DOA estimation with L-shaped array," *IEEE Signal Processing Letters*, vol. 21, no. 8, pp. 971–974, 2014.

[10] M. Yang, J. Ding, B. Chen, and X. Yuan, "Coprime L-shaped array connected by a triangular spatially-spread electromagnetic-vector-sensor for two-dimensional direction of arrival estimation," *IET Radar, Sonar & Navigation*, vol. 13, no. 10, pp. 1609–1615, 2019.

[11] G. Qin, Y. D. Zhang, and M. G. Amin, "DOA estimation exploiting moving dilated nested arrays," *IEEE Signal Processing Letters*, vol. 26, no. 3, pp. 490–494, 2019.

[12] F. Chen, J. Dai, N. Hu, and Z. Ye, "Sparse Bayesian learning for off-grid DOA estimation with nested arrays," *Digital Signal Processing*, vol. 82, pp. 187–193, 2018.

[13] Y. Wang, A. Hashemi-Sakhtsari, M. Trinkle, and B. W. H. Ng, "Sparsity-aware DOA estimation of quasi-stationary signals using nested arrays," *Signal Processing*, vol. 144, pp. 87–98, 2018.

[14] F. G. Yan, S. Liu, J. Wang, M. Jin, and Y. Shen, "Fast DOA estimation using co-prime array," *Electronics Letters*, vol. 54, no. 7, pp. 409-410, 2018.

[15] J. Li, D. Jiang, and X. Zhang, "Sparse representation based two-dimensional direction of arrival estimation using co-prime array," *Multidimensional Systems and Signal Processing*, vol. 29, no. 1, pp. 35–47, 2018.

[16] T. Wu, Z. Deng, Y. Li, and Y. Huang, "Two-dimensional DOA estimation for incoherently distributed sources with uniform rectangular arrays," *Sensors*, vol. 18, no. 11, p. 3600, 2018.

[17] D. Su, Y. Jiang, X. Wang, and X. Gao, "Omnidirectional precoding for massive MIMO with uniform rectangular array—-part I: complementary codes-based schemes," *IEEE Transactions on Signal Processing*, vol. 67, no. 18, pp. 4761–4771, 2019.

[18] Q. Li, T. Su, and K. Wu, "Accurate DOA estimation for large-scale uniform circular array using a single snapshot," *IEEE Communications Letters*, vol. 23, no. 2, pp. 302–305, 2019.

[19] J. Xin, G. Liao, Z. Yang, and H. Shen, "Ambiguity resolution for passive 2-D source localization with a uniform circular array," *Sensors*, vol. 18, no. 8, p. 2650, 2018.

[20] R. M. Shubair, A. S. Goian, M. I. AlHajri, and A. R. Kulaib, "A new technique for UCA-based DOA estimation of coherent signals," in *2016 16th Mediterranean Microwave Symposium (MMS),*, pp. 1–3, Abu Dhabi, United Arab, 2016.

[21] D. H. Xu and J. W. Chen, "A novel DOA estimation for uniform circular arrays in correlated environment without interpolation, pp. 650–652, Yonago, Japan, 2006.

[22] C. P. Mathews and M. D. Zoltowski, "Eigenstructure techniques for 2-D angle estimation with uniform circular arrays," *IEEE Transactions on Signal Processing*, vol. 42, no. 9, pp. 2395–2407, 1994.

[23] C. P. Mathews and M. D. Zoltowski, "Performance analysis of the UCA-ESPRIT algorithm for circular ring arrays," *IEEE Transactions on Signal Processing*, vol. 42, no. 9, pp. 2535–2539, 1994.

[24] R. Goossens and H. Rogier, "A hybrid UCA-RARE/Root-MUSIC approach for 2-D direction of arrival estimation in uniform circular arrays in the presence of mutual coupling," *IEEE Transactions on Antennas and Propagation*, vol. 55, no. 3, pp. 841–849, 2007.

[25] G. Jiang, X. Mao, and Y. Liu, "Reducing errors for root-MUSIC-based methods in uniform circular arrays," *IET Signal Processing*, vol. 12, no. 1, pp. 31–36, 2018.

[26] Y. Wang, X. Yang, J. Xie, L. Wang, and B. W. H. Ng, "Sparsity-inducing DOA estimation of coherent signals under the coexistence of mutual coupling and nonuniform noise," *IEEE Access*, vol. 7, pp. 40271–40278, 2019.

[27] J. C. Hung, "Memetic particle swarm optimization scheme for direction-of-arrival estimation in multipath environment," *Journal of Intelligent & Fuzzy Systems*, vol. 34, no. 6, pp. 3955–3968, 2018.

[28] V. Dakulagi and M. Bakhar, "Smart antenna system for DOA estimation using single snapshot," *Wireless Personal Communications*, vol. 107, no. 1, pp. 81–93, 2019.

[29] A. Sharma and S. Mathur, "Comparative analysis of ML-PSO DOA estimation with conventional techniques in varied multipath channel environment," *Wireless Personal Communications*, vol. 100, no. 3, pp. 803–817, 2018.

[30] P. Lindgren, P. Valter, and R. Prasad, "Retracted article: Advanced business model innovation supported by artificial intelligence, deep learning, multi business model patterns and a multi business model library," *Wireless Personal Communications*, vol. 107, no. 4, pp. 2263–2263, 2019.

[31] B. Sun and Z. Dong, "Comparative study on the academic field of artificial intelligence in China and other countries," *Wireless*

Personal Communications, vol. 102, no. 2, pp. 1879–1890, 2018.

[32] Y. Yue, L. Cao, and Z. Luo, "Hybrid artificial bee colony algorithm for improving the coverage and connectivity of wireless sensor networks," *Wireless Personal Communications*, vol. 108, no. 3, pp. 1719–1732, 2019.

[33] B. G. Prakash, R. Sukumar, and C. Balasubramanian, "A swarm intelligence based clustering technique with scheduling for the amelioration of lifetime in sensor networks," *Wireless Personal Communications*, vol. 103, no. 4, pp. 3189–3207, 2018.

[34] N. I. Chaudhary, S. Zubair, and M. A. Z. Raja, "Design of momentum LMS adaptive strategy for parameter estimation of Hammerstein controlled autoregressive systems," *Neural Computing and Applications*, vol. 30, no. 4, pp. 1133–1143, 2018.

[35] W. U. Khan, Z. Ye, F. Altaf, N. I. Chaudhary, and M. A. Z. Raja, "A novel application of fireworks heuristic paradigms for reliable treatment of nonlinear active noise control," *Applied Acoustics*, vol. 146, pp. 246–260, 2019.

[36] I. Ahmad, H. Ilyas, A. Urooj, M. S. Aslam, M. Shoaib, and M. A. Z. Raja, "Novel applications of intelligent computing paradigms for the analysis of nonlinear reactive transport model of the fluid in soft tissues and microvessels," *Neural Computing and Applications*, vol. 31, no. 12, pp. 9041–9059, 2019.

[37] C. Onnen, R. Babuška, U. Kaymak, J. M. Sousa, H. B. Verbruggen, and R. Isermann, "Genetic algorithms for optimization in predictive control," *Control Engineering Practice*, vol. 5, no. 10, pp. 1363–1372, 1997.

[38] A. Kartci, A. Agambayev, M. Farhat et al., "Synthesis and optimizsssation of fractionassl-order elements using a genetic algorithm," *IEEE Access*, vol. 7, pp. 80233–80246, 2019.

[39] W. Zang, W. Zhang, Z. Wang, D. Jiang, X. Liu, and M. Sun, "A novel double-strand DNA genetic algorithm for multi-objective optimization," *IEEE Access*, vol. 7, pp. 18821–18839, 2019.

[40] S. S. Moghaddasi and N. Faraji, "A hybrid algorithm based on particle filter and genetic algorithm for target tracking," *Expert Systems with Applications*, vol. 147, no. 1, article 113188, 2020.

[41] Y. Zhou, Y. Wang, K. Wang et al., "Hybrid genetic algorithm method for efficient and robust evaluation of remaining useful life of supercapacitors," *Applied Energy*, vol. 260, article 114169, 2020.

[42] A. H. Halim and I. Ismail, "Combinatorial optimization: comparison of heuristic algorithms in travelling salesman problem," *Archives of Computational Methods in Engineering*, vol. 26, no. 2, pp. 367–380, 2019.

[43] L. Tang, B. Tang, L. Kang, and L. Zhang, "A novel task caching and migration strategy in multi-access edge computing based on the genetic algorithm," *Future Internet*, vol. 11, no. 8, p. 181, 2019.

[44] S. Paul and S. Das, "Simultaneous feature selection and weighting—An evolutionary multi-objective optimization approach," *Pattern Recognition Letters*, vol. 65, pp. 51–59, 2015.

[45] K. S. Rajesh, S. S. Dash, and R. Rajagopal, "Hybrid improved firefly-pattern search optimized fuzzy aided PID controller for automatic generation control of power systems with multi-type generations," *Swarm and Evolutionary Computation*, vol. 44, pp. 200–211, 2019.

[46] E. Emary, H. M. Zawbaa, A. E. Hassanien, and B. Parv, "Multi-objective retinal vessel localization using flower pollination search algorithm with pattern search," *Advances in Data Analysis and Classification*, vol. 11, no. 3, pp. 611–627, 2017.

[47] H. Gozde and M. C. Taplamacioglu, "Automatic generation control application with craziness based particle swarm optimization in a thermal power system," *International Journal of Electrical Power & Energy Systems*, vol. 33, pp. 8–16, 2011.

[48] H. Martin, Z. Ma, C. Schmittner et al., "Combined automotive safety and security pattern engineering approach," *Reliability Engineering & System Safety*, vol. 198, article 106773, 2020.

[49] A. Shakya, M. Mishra, D. Maity, and G. Santarsiero, "Structural health monitoring based on the hybrid ant colony algorithm by using Hooke–Jeeves pattern search," *SN Applied Sciences*, vol. 1, no. 7, p. 799, 2019.